EUROPEAN FUSION DEVELOPMENT AGREEMENT

EFDA–JET–PR(04)67

D. Stork, Yu. Baranov, P. Belo, L. Bertalot, D. Borba, J.H. Brzozowski, C.D. Challis, D. Ciric, S. Conroy, M.de Baar, P.de Vries, P. Dumortier, L. Garzotti, N.C. Hawkes, T.C. Hender, E. Joffrin, T.T.C. Jones, V. Kiptily, P. Lamalle, J. Mailloux, M. Mantsinen, D.C. McDonald, M.F.F. Nave, R. Neu, M. O' Mullane, J. Ongena, R.J. Pearce, S. Popovichev, S.E. Sharapov, M. Stamp, J. Stober, E. Surrey, M. Valovic, I. Voitsekhovitch, H. Weisen, A.D. Whiteford, L. Worth, V. Yavorskij, K-D. Zastrow and EFDA JET contributors

Overview of Transport, Fast Particle and Heating and Current Drive Physics using Tritium in JET plasmas

Overview of Transport, Fast Particle and Heating and Current Drive Physics using Tritium in JET plasmas

D. Stork[1], Yu. Baranov[1], P. Belo[2], L. Bertalot[3], D. Borba[2], J.H. Brzozowski[4], C.D. Challis[1], D. Ciric[1], S. Conroy[5], M.de Baar[6], P.de Vries[1], P. Dumortier[7], L. Garzotti[8], N.C. Hawkes[1], T.C. Hender[1], E. Joffrin[9], T.T.C. Jones[1], V. Kiptily[1], P. Lamalle[7], J. Mailloux[1], M. Mantsinen[10], D.C. McDonald[1], M.F.F. Nave[2], R. Neu[11], M. O' Mullane[1], J. Ongena[7], R.J. Pearce[1], S. Popovichev[1], S.E. Sharapov[1], M. Stamp[1], J. Stober[11], E. Surrey[1], M. Valovic[1], I. Voitsekhovitch[1], H. Weisen[12], A.D. Whiteford[13], L. Worth[1], V. Yavorskij[14], K-D. Zastrow[1] and EFDA JET contributors*

[1]Euratom/UKAEA Fusion Association, Culham Science Centre, Abingdon, OX14 3DB, UK.
[2]Euratom/IST Fusion Association, Lisboa, Portugal
[3]Associazione EURATOM-ENEA sulla Fusione, Frascati, Italy
[4]Alfven Laboratory, EURATOM-VR Asociation, Stockholm, Sweden
[5]Dept. of Neutron Res., Uppsala University, EURATOM-VR Association, Uppsala, Sweden
[6]FOM Instituut voor Plasmaphysica, Associate Euratom, Nieuwegein, The Netherlands
[7]LPP-ERM/KMS, EURATOM-Belgian State Association, Brussels, Belgium
[8]Consorzio-RFX, Associazione EURATOM-ENEA sulla Fusione, Padova, Italy
[9]Association EURATOM-CEA sur la Fusion, CEA Cadarache, St Paul-lez-Durance, France.
[10]Helsinki Univ. of Technology, Association EURATOM-TEKES, Finland.
[11]Max-Planck Institut fur Plasmaphysik, EURATOM Assoziation, Garching, Germany
[12]CRPP, Association EURATOM-Confédération Suisse, Lausanne, Switzerland
[13]Dept. of Physics, University of Strathclyde, Glasgow, UK
[14]Inst. for Theoretical Physics, Univ. of Innsbruck, Association EURATOM-OEAW, Austria.
See appendix of J. Pamela et al., "Overview of JET results", in Proc of 19th IAEA Fusion EnergyConference, Lyon, 2002 (IAEA, Vienna, 2003) Partner in the Trilateral Euregio Cluster (TEC)*

Preprint of Paper to be submitted for publication in
Nuclear Fusion

ABSTRACT

Results are presented from the JET Trace Tritium Experimental (TTE) campaign using minority tritium (T) plasmas (n_T/n_D<3%). Thermal tritium particle transport coefficients (D_T, v_T) are found to exceed neo-classical values in all regimes, except in ELMy H-modes at high densities, and in the region of Internal Transport Barriers (ITB) in Reversed shear plasmas. In ELMy H-mode dimensionless parameter scans, at q value (q_{95} ~ 2.8) and triangularity (δ = 0.2), T particle transport scales in a Gyro-Bohm manner in the inner plasma (r/a<0.4), whilst the outer plasma particle transport behaves more like Bohm scaling. Dimensionless parameter scans show contrasting behaviour for trace particle confinement (increases with collisionality ν^* and β) and bulk energy confinement (decreases with ν^* and independent of β). In an extended ELMy H-mode dataset, with ρ^*, ν^*, β and q varied, but with NTMs either absent or limited to weak, benign core modes (4/3 or above) the multiparameter fit to the normalised diffusion coefficient in the outer plasma (0.65 < r/a < 0.8) gives $D_T/B_\phi \sim \rho^{*-2.46} . \nu^{*-0.23} . \beta^{-1.01} . q^{2.03}$. In hybrid scenarios ($q_{min}$~1, low positive shear, no sawteeth), T particle confinement is found to scale with increasing triangularity and plasma current. Comparing regimes (ELMy H-mode, ITB plasma, and Hybrid scenarios) in the outer plasma region, a correlation of high values of D_T with high values of v_T is seen. The normalised diffusion coefficients for the Hybrid and ITB scenarios do not fit the scaling derived for ELMy H-modes. The normalised tritium diffusion scales with normalised poloidal Larmor radius ($\rho_\theta^* = q\rho^*$) in a manner close to Gyro-Bohm (~ρ_θ^{*3}), with an added inverse β dependence. The effects of ELMs, sawteeth and Neo-classical Tearing Modes (NTMs) on T particle transport are described. Fast-ion confinement in Current-Hole (CH) plasmas, was tested in TTE by injection of Tritium NBI into JET CH plasmas. γ-rays from the reactions of fusion alphas and beryllium impurities ($^9Be(\alpha,n\gamma)^{12}C$) characterised the fast fusion-alpha population evolution. The γ-decay times are consistent with classical alpha plus parent fast triton slowing down times ($\tau_{Ts}+\tau_{\alpha s}$) for high plasma currents (I_p >2MA) and monotonic q-profiles. In CH discharges the γ-ray emission decay times are much lower than classical ($\tau_{Ts}+\tau_{\alpha s}$), indicating alpha confinement degradation, due to orbit losses and particle orbit drift predicted by a 3-D Fokker Planck numerical code, and modelled by TRANSP.

1. INTRODUCTION

The JET Tokamak is the only magnetic confinement fusion device currently having the capability of operating with deuterium-tritium (D-T) plasmas, including Tritium Neutral Beam Injection (NBI). D-T plasmas with concentration ratios in the range 10:90 < T:D < 90:10 have been exploited in previous campaigns studying fusion plasma phenomena [1,2]: including the generation of fusion power up to 16MW; the demonstration of alpha-particle heating in high performance regimes; and scaling of the ELMy H-mode behaviour of D-T plasmas towards ITER. Tritium is also useful in the study of particle transport. The evolution of the tritium spatial distribution can be detected in “trace” quantities (typically $n_T/(n_D+n_T)$<3% is used in experiments) by observation of the 14MeV neutron emission, allowing non-perturbative transient experiments using a fuel ion species. Thus, “trace

tritium" experiments allow the tritium convective velocity (v_T) and the diffusion coefficient (D_T) to be measured separately, in conditions where the bulk plasma parameters are in steady state. This is unlike particle transport studies on deuterium ions in steady-state plasmas, where only the ratio v_D/D_D, can be measured, and there are significant problems of source identification and ion density measurement. There are of course possibilities to evaluate the D_D and v_D separately in *perturbative* experiments such as those involving modulated gas puffing, but these have uncertainties on the precise values of the bulk plasma conditions under which the measurements are made. Previous 'trace tritium' experiments have been conducted on JET in 1997 [3, 4] and on TFTR [5, 6].

The JET Trace Tritium Experimental (TTE) campaign, reported in this paper, took place in September – October 2003, and whilst the core of the campaign focussed on particle transport, many other physics issues were addressed. The campaign featured experiments on: thermal particle (fuel ion) transport in a number of regimes and scenarios; fast ion transport and confinement; effects of MHD phenomena on thermal and fast-ion transport; and Ion Cyclotron Resonance Heating (ICRH) of tritium minority species. This paper gives an overview of results in the first three of these fields and indicates work still in progress. The campaign also produced significant results in development of 14MeV neutron diagnostics. These are reported in reference [7].

2. GENERAL EXPERIMENTAL CONDITIONS

Technical details of the systems involved in the TTE Campaign are given in [8]. Tritium was introduced into JET by short, 80ms, T_2 gas puffs of ≤ 6mg, or by short (typically 200ms) pulses with T^0-NBI (~100keV, 1MW). The time evolution of the tritium gas source entering the plasma was accurately measured locally with 10ms time resolution from T_α emission on a line-of-sight local to the inlet valve. The detailed shape of the gas flow could be measured in L-mode discharges and was established as invariant in all discharges where it was measured, giving an accurate time-stamp for the start of the tritium transport data, which is required for accurate transport analysis (see section 3). Following the gas puff, about 10% of the tritium puffed was found inside the plasma by the time of peak neutron emission (in contrast to T^0-NBI which has near 100% fuelling efficiency). The rest of the tritium gas after the puff was in the vessel wall and divertor tiles. Tritium released from these components acted as a source and could affect the transport results (see below). To minimise the effect, frequent 'clean-up' pulses were run in pure D-D plasmas, keeping the tritium wall inventory to a minimum.

The ratio of tritium ions to deuterium ions ($n_T/(n_D+n_T)$) in the TTE plasmas was monitored throughout the campaign using Silicon diode detectors [9] which measured the integrated yields, within a shot, of 2.5MeV neutrons (from DD reactions) and 14MeV neutrons (from DT reactions). The history of tritium concentration throughout the campaign can be seen in Fig.1, where the intermittent D-D clean-up periods are evident. Also plotted on the figure is the prediction of an empirical model based on the amount of fuelling (minority tritium and majority deuterium). This

model is based on one derived during the first JET tritium experiment, the Preliminary Tritium Experiment (PTE) [1], which was applied to the later JET 'DTE1' campaign [10]. For the TTE campaign, it was found that the tritium removal'*from those wall reservoirs which exchange with the plasma* was more accurately predicted if the scaling according to D_2 fuelling was included by:

$$f_T(n) = \sum_{j=1}^{n-1} \frac{Q_j^T}{Q_0^T} F\left(\sum_{i=j}^{n-1} \frac{Q_i^D}{Q_0^D} \right) \tag{1}$$

where $f_T(n)$ is the tritium fraction in the plasma in the *nth* pulse of the Campaign (which starts with a pulse with $Q_1{}^T$ tritium atoms), and F(m) is a dilution function describing the background tritium level in the *mth* pulse, with deuterium fuelling $Q_m{}^D$ atoms, following the introduction of $Q_j{}^T$ tritium atoms in the *jth* pulse of the Campaign. $Q_0{}^T$ and $Q_0{}^D$ are normalising constants of the model.

Over the whole TTE Campaign, a total of 380mg of tritium gas was puffed into over 80 JET plasma pulses. The tritium NBI into the plasmas amounted to an integrated time of 20 beam-seconds spread over 74 further JET pulses. The integrated 14MeV neutron yield for the campaign was 4 10^{18} neutrons.

The neutron emission from DD and DT reactions was measured spatially with a nineteen-channel neutron profile monitor [11]. The profile monitor has ten horizontal and nine vertical lines-of-sight; these are overlayed on the emissivity contours shown in Fig.2. All channels are absolutely calibrated at 2.5MeV for DD and 14MeV for DT reactions, and provide 10ms time resolution.

The outermost channels of the camera with good statistics were channels #9(horizontal) and #19(vertical), with typically r/a=0.82. Thus valid particle transport results were obtained in the TTE Campaign for the plasma inside r/a≈0.85.

3. THERMAL PARTICLE TRANSPORT ANALYSIS AND RESULTS

The TTE Campaign produced data that enables investigation of several aspects of thermal particle transport: fuel-ion particle transport dimensionless-parameter scaling in ELMy H-modes; fuel-ion particle transport in various ELMy H-modes scenarios – high vs low density, plasmas with high ICRF heating, impurity-seeded discharges; effects of sawteeth and ELMs on fuel-ion transport; fuel-ion transport in Internal Transport Barrier (ITB) and hybrid scenarios; and confinement effects on thermal ions of Neo-classical Tearing Modes (NTMs).

3.1 GENERAL ANALYSIS METHOD

The thermal particle transport analysis parameterises the transport of tritons in an advection/diffusion model:

$$\frac{\partial n_T}{\partial t} = -\frac{1}{r} \cdot \frac{\partial}{\partial r}\left(r\Gamma_T\right) + \sigma\left(t\right) \tag{2}$$

$$\Gamma_T = -D_T \cdot \frac{\partial n_T}{\partial r} + v_T \cdot n_T \tag{3}$$

Where the subscript 'T' refers to tritons; Γ_T represents a flux of tritons; $\sigma(t)$ is the time dependent triton source; and D_T and v_T are the triton diffusion coefficient and convective velocity respectively.

Data from selected channels of the 14MeV neutron profile monitor are shown in Fig.3(a). Following the tritium puff, the 14MeV signal rose on all channels as the tritium ions diffused inward. During this rise phase, the data are used to derive values for D_T and v_T. In the following phase, once the tritium ion profiles were centrally peaked, the gradients drove the ions from the plasma, and during this relaxation, only the ratio v_T/D_T can be determined as a cross-check. As the tritium gas puff did not perturb plasma parameters, the transport coefficients are assumed to be constant in time for ELMy H-Mode and hybrid scenario discharges, whereas radial movement of transport barriers is allowed for ITB discharges. The details of the least-squares fitting of data from the neutron profile monitor and neutron yield with a transport model for tritium with free parameters for the spatial profiles of D_T and v_T and the influx are given in reference [12]. The modeling includes neutral transport and losses from charge exchange with cold neutrals and fast beam neutrals. The tritium ion density, is calculated using the SANCO $1^1/_2$–D impurity transport code [13], and processed using the TRANSP code [14] obtaining coefficients relating to the 2D emissivity profile to the line-of-sight integrals obtained by the neutron camera [12]. D_T and v_T are obtained by the best least-squares fit to the 19-channel neutron time history data is. The least squares fitting and post-processing are performed by the transport analysis package UTC [15]. The majority of discharges in which thermal particle transport was studied were performed in matched pairs, one with tritium gas puff and one with a short pulse of T° NBI into identical conditions. As indicated in section 2, in the gas puff shots the majority of the tritium went straight to the walls and divertor. This tritium was released later in the shot as a result of energetic loss processes (eg:ELMs), and affected the decay rate of tritium seen on the 14MeV neutron signal. The T° NBI shots were not prone to this delayed source and hence their tritium content decayed much faster once the T^+ fast ions had thermalised. The decay rate in these shots was used as the consistency check on v_T/D_T derived from the gas puff shots. As will be shown in section 4, comparison of the relative plasma tritium content decay rates in the NBI and gas puff cases also yields data on fuelling efficiency and wall residence time.

3.2 ELMY H MODE RESULTS

The fits to the data show that tritium transport exceeds neo-classical levels in most ELMy H-mode cases studied, only approaching neo-classical levels in ELMy H-modes at high densities near the Greenwald limit (see Fig.3(b)). For the majority of the ELMy H-mode dataset, and for all the ELMy H-modes discussed in this section, strong NTMs were absent, with NTM activity being limited to weak higher order (4/3 and 5/4) modes in the plasma core. Almost all these discharges had sawteeth however. The transport coefficients discussed in this section are averaged over the occurrence of sawteeth and ELMs. The effects of these discrete MHD phenomena are discussed below in Section 4. Over the ELMy H-mode dataset a strong inverse correlation of the anomalous

tritium transport with plasma density is found: the D_T is close to its neoclassical value (as predicted using the NCLASS code [16]) at high density whilst the diffusion is strongly anomalous at low density. Likewise the tritium pinch (v_T) is closer to the neoclassical one in high density plasma, but it becomes highly anomalous at low density. As can be seen in the high density shot portrayed in Fig.3(b), the measured D_T remains above neo-classical in the outer part of the plasma (r/a > 0.6), but agrees with neo-classical predictions within r/a < 0.5. The thermal effective diffusivity does not display such strong density dependence leading to the density dependent ratio χ_{eff}/D_T. [17].

Dedicated 'dimensionless variable' scans were also performed to study tritium transport in NBI-heated, low q (q_{95} = 2.8), low triangularity (δ=0.2) ELMy H-modes. The details are given in reference [18].

Scans were performed in each of ρ^* (Ion Larmor radius normalised to minor radius), ν^* (normalised collisionality ~ naq/T_e^2) and β (normalised plasma pressure), with the remaining two variables held approximately constant over the scan. The results showed that a strong 'Gyro-Bohm' like dependence on ρ^* in the inner part of the plasma ($D_T/B_\phi \propto \rho^{*3.22\pm0.62}$, for 0<r/a<0.45) with a weaker 'Bohm' like dependence in the outer part of the plasma ($D_T/B_\phi \propto \rho^{*1.9\pm0.38}$, for 0.6<r/a<0.85). For the ν^* and β dependence the following fits are obtained:

$$D_{T,inner}/B_\phi \propto \beta^{-0.34\pm0.08}; \quad D_{T,outer}/B_\phi \propto \beta^{-0.55\pm0.09};$$
$$D_{T,inner}/B_\phi \propto \nu^{*-0.51\pm0.17}; \quad D_{T,outer}/B_\phi \propto \nu^{*-0.40\pm0.15} \qquad (4)$$

The β and ν^* dependences for D_T are in strong contrast to the energy confinement scalings in the scans [18]: the energy confinement is largely independent of β, whilst the dependence on ν^* is actually in the opposite sense to particle confinement, with energy confinement decreasing weakly as ν^* increases. These results for ν^* are consistent with the density dependence seen generally in the χ_{eff}/D_T ratio.

The dataset of NBI heated ELMy H-modes is wider than the data from the 'dimensionless variable 'scans'. The addition of other NBI-heated ELMy H-modes without strong NTMs increases the dataset to nine discharges and introduces a variation in q. If this data is fitted then the normalized diffusion coefficients for the plasma region 0.65 <r/a <0.8 show the following dependence (displayed in Fig.4):

$$D_T / B_\phi \propto \rho^{*a_\rho} \cdot \nu^{*a_\nu} \cdot \beta^{a_\beta} \cdot q^{a_q} \qquad (5)$$

where $a_r = 2.46 \pm 0.2$
$a_n = -0.23 \pm 0.05$
$a_b = -1.01 \pm 0.08$
$a_q = 2.03 \pm 0.17$

Although the coefficients for the variation of ρ^*, ν^*, β have changed from the more restricted

dataset of equations (4), the basic β and v^* dependences of the diffusion coefficient are maintained and remain in strong contrast to the energy confinement scaling. It is notable that a similar inverse β-dependence was found on DIII-D for helium particle transport [19].

3.3 HYBRID SCENARIO RESULTS

Following the development in ASDEX-Upgrade [20] and DIII-D [21] of plasmas with q_{min}~1, low positive shear, and no sawteeth in the so-called 'Hybrid' scenarios such discharges have been investigated on JET [22]. For these discharges the tritium transport following gas puffs and T^0 NBI was studied. The plasma triangularity was scanned (δ = 0.2 - 0.46), at approximately constant gain factor G ($G=H_{89}\beta_N/q_{95}^2 \sim 0.32$). The data was compared in two complimentary ways. The raw decays of 14MeV neutron signal following thermalisation of tritium fast ions from NBI, where wall sources were negligible, showed a global improvement in T particle confinement time (τ_{pT}^*) by ~ 50% over the scan. In addition, fits were performed to the 14MeV neutron signals following tritium gas puffs into identical discharges. The results are shown in Fig.5. The improvement in τ_{pT}^* is found to be explained in terms of a reduction in D_T across the whole plasma (although errors on the fits reduced the significance of this for r/a >0.5), whilst the values of v_T are independent of d. In addition, I_p and B_T were varied at constant q_{95} and low δ. The neutron decay following T^0 NBI shows τ_{pT}^* scaled with $I_{p,}$ and the detailed fits in the gas puff shots show that the change is explained by a reduction in D_T confined to r/a > 0.5, although with less statistical significance than the changes seen in the triangularity scan. Again the fitted values of v_T are independent of I_p, B_T. In all cases the fitted values of D_T and v_T are once again considerably above the neoclassical predictions.

3.4 INTERNAL TRANSPORT BARRIER (ITB) DISCHARGE RESULTS

In ITB discharges with a strong single barrier [23], three features are observed: a reduction of D_T to neo-classical values in the transport barrier; an increase of D_T to large values in the region within the barrier; and a reduction of v_T in the barrier, see Fig.6(c). The absolute value of v_T within the barrier remains above neo-classical values. The reduction of D_T in the barrier impedes tritium from reaching the core, whilst the increased D_T in the region enclosed by the barrier speeds up both the rate of rise to peak emission, and the decay rate after the peak emission seen by the innermost channels in agreement with the line integrals measured by the cameras. Details of tritium transport with ITBs present are given in [24].

3.5 TRITIUM FUELLING RESULTS

ELMy H-modes have been used to investigate the causes behind the global gas-fuelling efficiency. Of order 90% of the tritium after a gas puff is in or on the vessel wall and divertor tiles. Tritium released from these components acts as a fuel source and is responsible for the observed delay of tritium decay from the plasma. For the analysis of tritium ion transport a simple model for the flux in and out of the region observed by the neutron diagnostic has been used with a quasi-realistic

three-reservoir model (plasma, wall, divertor). The equations for rate of change of tritium content in these reservoirs are:

$$dN_{TW}/dt = x\Gamma - N_{TW}/\tau_{WT} \quad (6)$$

$$dN_{TP}/dt = f_{SOL}\ f_{D,V}\ [(1-x)\Gamma + N_{TW}/\tau_{NT}] + \varepsilon N_{TD} - N_{TP}/\tau_{PT} \quad (7)$$

$$dN_{TD}/dt = (1 - f_{SOL}\ f_{D,V})\ [(1-x)\Gamma + N_{TW}/\tau_{NT}] - \varepsilon N_{TD} + N_{TP}/\tau_{PT} - N_{TD}/\tau_{DT} \quad (8)$$

where N_{TW}, N_{TP}, N_{TD} are the tritium atom (ion) content in the wall, plasma and divertor tiles respectively;

τ_{WT}, τ_{PT}, τ_{DT} are the tritium residence times in the wall, plasma and divertor tiles;

G is the flux of tritium atoms from the gas valve;

f_{SOL} is the probability of a tritium ion penetrating the scrape off layer ($_{SOL}$)

$f_{D,V}$ is the probability of tritium ion penetrating through to the region seen by the neutron cameras (r/a <0.85) – a function of *D* and *v*;

ε is the fuelling efficiency from the divertor

x is the fraction of the gas puff going directly to the wall

Equation (8) is effectively solved by noting

$$N_{TD}(t = \infty) = \int \Gamma dt - N_{TW} - N_{TP} \quad (9)$$

Equation (7) is solved by the SANCO code to get N_{TP} from the 14MeV neutron signal. In this process we set the value of τ_{PT} equal to the decay time in the accompanying T° NBI discharge, and $f_{SOL} = 1$.

Results using this model yield physically plausible values for the free parameters: the fraction of tritium going direct to the wall was x ~ 0.6 (simple arguments of molecular breakup in the scrape-off layer would give ~ 0.5), and typical wall retention times τ_{WT} ~ 0.3 -0.5s. are found (of the order of the plasma energy confinement time). The divertor retention time is longer than 5s. The gas fuelling efficiency data thus yields a picture in which: around 60% of the gas goes direct to the wall, and is then desorbed easily by the plasma heat efflux on an energy confinement scale; and ~ 30% is transported quickly out of the outer region (r/a > 0.85), and deposited in the divertor, with a much longer characteristic timescale for return.

The data on ITB discharges have been interpreted to give preliminary results on the relative fuelling efficiency of tritium gas puffing, tritium recycled from the walls and T^0 NBI. Fig.7(a) shows ion temperature (T_I) and electron density (n_e) profiles for three identical ITB discharges with a single strong barrier, the tritium fuelling being supplied by gas puff, T^0 NBI, and finally solely from wall recycling. The barrier measurements were made at suitable times (for the shot with T^0 NBI when the fast T^+ ions had thermalised, as calculated by the TRANSP code [14], for the gas puff shot when the tritium arrived in the core). The 14MeV neutron emissivities for the three discharges are shown in Fig.7(b). The ratio of the total tritium atoms injected during a gas puff to

that injected during the T^0 NBI pulse was ($3.1\ 10^{20}$ / $8.2\ 10^{18}$) ~ 38, whilst the ratio of the core emissivities in the two cases was ~1.6, indicating that T^0 NBI is ~ 25 times more efficient at core fuelling. For discharges with weaker ITBs, although the T^0 NBI is always more efficient, the difference is not as pronounced, indicating that the relative fuelling efficiency depends on confinement inside the plasma.

The ratio of 25:1 advantage for T^0 NBI over T_2 gas puffing in the core of ITB discharges compares to an approximate 10:1 advantage for an ELMy H-mode plasma globally, inferred from the ~10% of tritium found inside the plasma at peak neutron emission following a tritium gas puff. This indicates that there is a further barrier to fuelling the core presented by an ITB. Such fuelling considerations will be important in the transient phase of ITB scenarios used to start up burning D-T plasmas.

3.6 COMPARISON OF PARTICLE TRANSPORT IN DIFFERENT REGIMES

For a comparison of the scaling of transport in the different regimes studied, the analysis has focussed on the outer region observed by the neutron cameras, i.e. $0.65<r/a<0.8$. In the central region, differences between ELMy H-Mode discharges ($q_0<1$, exhibiting sawtooth behaviour), hybrid scenarios ($q_0\approx1$) and ITB discharges ($q_0>2$ or even $q_0>3$) can be expected. In contrast, tritium transport well outside the central region should be comparable between all scenarios.

For all regimes, high values of D_T correlate with high values of v_T. The ratio v_T/D_T, which determines the tritium profile shape, varies from $-3m^{-1}$ for high q, low density ELMy H-modes to $\pm 0.1\ m^{-1}$ at low q, high density. The ratios for the hybrid scenarios generally follow the ELMy H-mode, but the ITB discharges stand out with very high inward convective velocities (see Fig.8(a)). The higher inward convective velocities are not sufficient to offset the dominant effect of the faster diffusive tritium loss in all regimes. This applies up to values of $D_T \sim 4m^2 sec^{-1}$, as can be seen in the drop in global decay time (τ_{pT}*) of the tritium density (as measured by the loss of thermal tritons after thermalisation of a T° NBI pulse) shown in Fig.8(b). At higher values of D_T this decline in τ_{pT}^{*} seems to be reaching asymptotic values.

There is a strong correlation for all three scenarios of D_T with q_{95} (scanned by varying current and toroidal field) for $0.65<r/a<0.8$. Energy transport in the same discharges, characterized by χ_{eff}, is not strongly affected, and thus D_T/χ_{eff} varies between 0.3 (high density, low q_{95}) and 2.0 (low density, high q_{95}). Initial results show plasmas with added ICRH have a larger ratio of D_T/χ_{eff}, a phenomenon still under investigation. D_T correlates better with the local value of q, suggesting that the orbit width of trapped particles could be an important parameter determining the scaling. Fig.9 shows the relationship of the normalized diffusion coefficient D_T/B_ϕ [25] with the normalized poloidal Larmor radius $\rho^*_{pol} = q\times\rho^*$ (where $\rho^* \sim T_i^{1/2}/aB$). This results in a very strong correlation for the ELMy H-Mode discharges alone, which is better described by gyro-Bohm scaling (ρ^{*3}_{pol}) rather than Bohm scaling (ρ^{*2}_{pol}). Note how the inclusion of q in the scaling parameter has now altered the conclusion with respect to Gyro-Bohm/Bohm scaling reached in the dimensionless

parameter scans [18]. With ρ^*_{pol} as scaling parameter, differences appear for hybrid scenario discharges and for discharges with significant ICRH heating, whilst the two ITB discharges agree with the trend within errors. Fig.9 also shows an equally strong trend for v_T/B_ϕ with local ρ^*_{pol}. In this inset, the hybrid scenario discharges again follow the trend of the ELMy H-Mode discharges, whereas the ITB discharges stand out.

The hybrid scenario discharges are characterised by larger β, and the behaviour of D_T with β is consistent with the fits to ELMy H-mode data in the specific dimensionless parameter scans (described above).

Finally, the fitted values of D_T/B_ϕ for hybrid scenario discharges and ITB discharges are plotted on Fig.10 to compare with the multi-parameter fit derived for the outer region of the ELMy H-mode discharges (equation (5)). In general this multi-parameter fit does not provide a description of the hybrid and ITB data. It can be seen that the hybrid datapoints appear to divide into two groups: one close to the fitted line, the other significantly shifted. Examination of the dataset shows that it is the higher triangularity hybrid discharges which lie close to the fitted line, whilst the lower triangularity ($\delta = 0.2$) discharges are displaced. This is an odd result, as the lower value of triangularity is shared by the bulk of the ELMy H-mode dataset (except for the point at very low D_T/B_ϕ nearest the origin). Further analysis work to elucidate these effects is in progress. A refit of the dataset to the ELMy H-mode *plus* hybrid scenario discharges changes the exponents in the multi-parameter power law expression of equation (5) to $a_\rho = 2.64$; $a_\nu = 0.17$; $a_\beta = -1.26$; $a_q = 1.47$. The ρ^* and β dependencies are hence largely preserved, with the ν^* dependence changing sign but still being close to zero, whilst the q dependence is reduced. The grouping of the hybrid scenario discharges suggests however that applying this fit to the wider dataset may not be valid. An attempt to include the ITB discharges in the same manner deteriorates the quality of the fit still further, with only the exponent of β (a_β) remaining largely unaltered.

4. MHD EFFECTS ON THERMAL PARTICLE TRANSPORT

Sawtooth collapses resulted in tritium density-profile changes [17]. The dominant contribution to the observed changes of the neutron line integrals is the redistribution of fast NBI-derived deuterium ions. At the time when they disappeared from the central channels (evident from a dip in the central line integrals), a burst of 14MeV neutrons was seen in channels with an impact parameter as far as $r/a \approx 0.5$. Sawtooth collapses that occurred during inward propagation of tritium, i.e. shortly after the puff, did not exhibit this feature: the ejection of deuterium ions from the core being compensated by the tritium ions being swept into the core, keeping the line integrals almost constant. Sawtooth effects were most pronounced at low density, where the NBI deuterium ion density was more peaked.

ELMs that occured during the time of the puff resulted in a noticeable increase of 14MeV line integrals with an impact parameter as far into the plasma as $r/a \approx 0.5$ within 10ms. We do not have a quantitative understanding of this effect, but changes in ELM frequency should result in changes

to the fuelling efficiency of tritium on the assumption that D_T during an ELM rises significantly above the level of D_T between ELMs [26]. The transient effects could be the result of deeper fuelling due to charge-exchange as a result of the increase of the deuterium neutral flux after the ELM, but note that simultaneously losses due to charge-exchange would also increase, leading to a null effect. It is also possible that tritium neutral influx increases as a result of energy or particles released from the plasma during the ELM, dislodging tritium from the wall or divertor. The combination of all three effects will require further analysis to elucidate.

The effect of strong NTMs was studied in pairs of discharges with near identical plasma conditions, one with and one without a 3/2 NTM [27] as shown in Fig.11. Changes to 14MeV line integrals were observed for lines-of-sight with an impact parameter inside the region of q<3/2, with channels outside the q = 3/2 surface being little affected. It can be clearly seen from the 14MeV neutron emission (Fig.12) that shots with NTMs show more rapid transit of tritium to the plasma centre. Analysis also demonstrates that there is a more rapid decay of the tritium density profile after peaking. Allowing for the slight differences in temperature and density between the discharges, the major part of the changes require a change in the tritium transport, localized at, or within, the q=3/2 surface. Both changes in D_T and v_T are consistent with the observations, but the effect of the NTM on fast ions (which mainly determine the neutron emission in this region) requires further modelling to reach a firm conclusion.

5. FAST PARTICLE TRANSPORT

Tritium NBI ions were used in several fast particle transport experiments. The confinement of tritium beam-ions was studied in reversed-shear (ITB) and 'current-hole' plasmas. The effect of Toroidal Alfven Eigenmode (TAE) and Fishbone modes on fast T ion transport was also studied. For diagnosis of the alpha particles (α) produced in the D-T reactions the diagnostic method based on g-rays from the $^{9}Be(\alpha,n\gamma)^{12}C$ nuclear reaction was used. During TTE the slowing down of fusion born alphas was measured for the first time with this approach, using a well shielded high-efficiency γ ray spectrometer based on a bismuth germanate (*BGO*) detector [28].

In JET plasmas with a Current Hole (CH) the toroidal current density falls to near zero for typically 30-40% of the minor radius [29], and there is an ITB near the edge of the CH. These plasmas are expected to confine fast ions poorly as a result of the very low central poloidal field (B_q). The effect of a CH on fast beam ions was demonstrated by measuring the 14MeV neutron profiles from the interactions of 105kV triton beam ions with the background deuterium. As the D-T reactivity (σv_{DT}) decreases rapidly with triton energy, the information covers the fast triton behavior in a narrow energy range E_b-E<<E_b, (where E_b= 105kV). Tritons were injected into both CH and Monotonic Current profile (MC) plasmas with the same plasma current (1.5 – 2MA), and the triton beams were injected both on and off the magnetic axis (in the vertical dimension). The poloidal plane projections of the injected orbits are shown in Fig.13. For on-axis injection, the measured neutron profiles demonstrate an outward shift induced by the CH (Fig.14(a)) whilst for off-axis tritons (not shown) the peak is shifted inwards.

The behavior of the fast beam tritons has been modelled with a 3-D Fokker-Planck code [30], and also in TRANSP [31]. For individual tritons, consideration of the orbits shows that the maximum ion density corresponds to a mid-plane radius where beam tritons execute near-'stagnation' orbits, with radial (v_r) and vertical (v_z) drift velocities near zero. For fast triton ions born near the magnetic mid-plane (z = 0), the motion along field lines results in a vertical drift $v_z = v_{//} B_z / B$. This drift is opposed by the curvature and ∇B drifts such that:

$$v_z = - v_d + v_{//} B_z / B = 0 \qquad (9)$$

with v_d the sum of curvature and ∇B drifts:

$$v_d = (v_{//}^2 + \tfrac{1}{2} v_{\perp}^2) / \omega_c R \qquad (10)$$

The equality of condition (9) leads to the trapping of the triton at the mid-plane and to the locally enhanced fast ion density that, in principle, can be detected as a peak in the 14MeV neutron emission. Equation (9) can only apply exactly at the mid-plane, as otherwise there are radial drifts ($v_r = v_{//} B_r / B_0$). In addition the cross-field (curvature and ∇B) drifts are relatively weak and hence the stagnation condition is only realized at low pitch angles. In CH plasmas however, there is an extended region of low poloidal field, B_θ ($B_\theta = B_z$ at z = 0) and this gives rise to an outward radial extension to the stagnation point [29]. This outward shift in the stagnation point leads to a detectable outward shift in the peak of the 14MeV neutron profile, as seen in Fig.14(a).

The results of the 3-D Fokker Planck model show a satisfactory explanation for the measured 14MeV profiles. As an example, Fig.14(b) shows the modelled profiles for on-axis triton beam injection into a CH plasma, which compare qualitatively with the data. The TRANSP modelling also shows qualitative agreement (Fig.14(c)). The centroid of the neutron distribution was measured by averaging the yields in the camera inner channels. This centroid was seen to move as the edge of the CH region, as established by the MSE diagnostic [31], moved with the current profile evolution. Occasionally, the CH was instantaneously eroded by MHD activity, and in these cases a corresponding step change in the neutron profile centroid was seen (Fig.15).

During TTE the first diagnostic measurements of γ-rays produced from populations of fusion α-particles were performed. The decay rates of γ-rays from reaction $^9Be(\alpha,n\gamma)^{12}C$ following T^0 NBI pulses were measured in many TTE discharges. This decay rate can be related to the combined slowing down of the parent beam tritons ($\tau_{SD,T}$) and the alphas ($\tau_{SD,\alpha}$) subsequently produced [28]. Here the value of $\tau_{SD,\alpha}$ is understood as the time for an α-particle to slow down from its birth energy (centred on 3.5MeV, dependent on the velocity of the beam triton) to the γ-detector threshold energy at 1.7MeV [28], and the value of $\tau_{SD,T}$ signifies the time for a triton to slow down from injection energy (~105keV) to an energy where the cross section for α-particle production has dropped by a factor $\sim e^{1.0}$ (approximately 70keV). The combined value of ($\tau_{SD,T} + \tau_{SD,\alpha}$) can be compared to the measured γ decay, as in Fig.16. In discharges with relatively high monotonic

currents (I_p>2MA) the observed density decay of fast ions inferred from γ-ray measurements was consistent with, or longer than, classical slowing down, while in 2.5MA discharges with a current hole as large as about 1/3 of the plasma radius the measured decay time was much shorter than the classical slowing down time, indicating confinement degradation or radial transport of fast alphas similar to that seen at low current (I_p=1MA). The confinement of charged fusion products (CFPs) has been modelled with the 3D Fokker-Planck (F-P) code in reversed shear plasmas in the axi-symmetric limit [30]. The 3-D code takes into account the combined effects of alpha loss and transport out of the detector line-of-sight. A strong effect of reversed shear on CFP confinement is found when the plasma current is less than the critical current, I_{cr}, required to confine the fattest bananas crossing the plasma core [32]. I_{cr} increases with the size of the "zero" poloidal field region, r_*/a, and for typical JET CH discharges exceeds 4MA for 3.5MeV alphas if r_*/a > 0.4. In MC plasmas, this critical current, I_{cr}, is of order 2MA. The confinement of CFPs in CH discharges (strong RS) with r_*/a > 0.4 is significantly degraded compared to MC plasmas even at relatively high plasma currents I_p=2-2.5MA. For low currents, where I_p<I_{cr}, strong RS results in a substantial reduction of the density of fast CFPs due to confinement degradation and spatial redistribution both effected by the ion orbit topology modification. Calculated rates of decay of γ-ray production by fusion alphas, as seen along the γ-ray spectrometer observation line of sight in JET, are displayed in Fig.17. The case with large CH at I_p = 2.5MA correponds to a TTE Pulse No: 61340 with measured $T_e(0)$ = 8.4keV and $n_e(0)$ = 3.8 10^{19} m^{-3}. Other curves compare postulated plasmas with the same T_e and n_e profiles but MC profiles. The reductions in γ-rate, and in γ-decay time for the CH case are clearly seen. Thus, in agreement with experiment, and TRANSP simulations (Fig.17), the 3D F-P code shows that RS decreases the decay time of the fast alpha distribution.

The evolution of T^+ fast ions from T^0 NBI with velocities comparable to the Alfven velocity was investigated in TTE discharges with B_T=0.86 T, I_p=0.9 MA. The deuterium (D^0) NBI was used at power levels > 5MW to destabilise TAE and n=1 Fishbones. The 14MeV neutron camera profiles' evolution was measured during four 50ms pulses of T^0 NBI injected on top of the D^0 heating. The effects of fishbones were seen, as loss of central fast ions, on the T^0 NBI deposition profiles: although these effects were not as large as those observed in earlier JET 10:90 D-T plasma experiments [33], at higher powers and similar plasma current and q. No appreciable effect was found for low amplitude TAEs. Details of the experiment are given in ref [34].

CONCLUSIONS

The TTE Campaign has demonstrated the usefulness of trace tritium plasmas in deriving information on the thermal fuel-ion and fast ion particle transport. The tritium particle transport coefficients (D_T, v_T) were measured successfully in three regimes of interest to ITER (ELMy H-mode, Hybrid scenario and ITB plasmas), although work is still in progress, several conclusions can already be drawn.

i) The values of D_T and v_T were found to be substantially in excess of neo-classical values in all

regimes except for high density ELMy H-modes near the Greenwald density limit and ITB plasmas in the region of the Transport Barrier itself.

The strong density variation of D_T in ELMy H-modes is not followed by the effective thermal diffusivity, χ_{eff}, leading to a density dependent D_T / χ_{eff} ratio, varying from $0.3 < D_T / \chi_{eff} < 3.0$, in strong contrast to what is normally assumed in ITER predictions [35, 36].

ii) The tritium normalized diffusion coefficient (D_T/B_ϕ) shows a mixed Gyro Bohm/Bohm scaling when the behaviour in dimensionless parameter scans is studied in ELMy H-modes. For the central plasma ($0 < r/a < 0.4$) the scaling is Gyro Bohm-like ($\sim\rho^{*3}$) whilst in the outer part of the plasma ($0.65 < r/a < 0.8$) the behaviour is more Bohm-like ($\sim\rho^{*2}$).

iii) The tritium particle transport in ELMy H-modes shows a strong inverse β dependence, with D_T/B_ϕ scaling between $\beta^{-0.5}$ and β^{-1} depending on the collection of parameters used in the fit, the region of the plasma to which the fit is applied, and the class of discharges used in the fit. This is very different to the behaviour of energy confinement [18]. The behaviour with ν^* is less pronounced, but the weight of evidence points to mild inverse ν^* dependence in all plasma regions. This ν^* dependence is consistent with the density behavior established for D_T. Again there is a contrast with the energy dependence established for ELMy H-modes.

iv) In hybrid scenarios, increasing triangularity and plasma current raises tritium particle confinement, but transport remains in excess of neo-classical values.

v) All three regimes show a strong dependence of D_T on the local safety factor (q) in the outer region of the plasma ($0.65 < r/a < 0.8$). For ELMy H-modes this can be expressed by an approximate q^2 dependence. The multi-parameter fit to the ELMy H-mode dataset (equation (5)) is not followed by the Hybrid or ITB discharges, which exhibit lower particle diffusion at the same values o the dimensionless parameter set (ρ^*, ν^*, β and q). Bringing the Hybrid discharges into the fitted dataset does however largely preserve the dependence on ρ^* and β, indicating that there are some common underlying trends between ELMy H-modes and Hybrids, as might be supposed from their common origin.

vi) All three regimes show a correlation between high values of D_T and high values of v_T.

vii) The strong dependence on q and ρ^* has led us to compare the dependence of the particle transport parameters on the *Poloidal* gyroradius, $\rho_{pol}{}^*$ ($= q \times \rho^*$). For the outer regions of the plasma this is only partially successful (given the spread in β amongst the fitted plasmas) but a Gyro Bohm-like dependence ($D_T / B_\phi \sim \rho_{pol}{}^{*3}$) is seen for ELMy H-mode plasmas.

viii) The effects of sawteeth, ELMs and strong 3/2 NTMs can all be seen on the 14MeV neutron profiles and, by inference, on the tritium transport. In the case of the 3/2 NTMs, the effects are confined within the NTM location (i.e. within $q = 3/2$ surface) and are found to deteriorate the particle confinement.

The effects of a Current Hole in the centre of JET plasmas on fast injected NBI ions can be seen as outward shifts in the deposition profile for on-axis injection. This is qualitatively explained both by 3-D Fokker Planck numerical code and by TRANSP modelling. γ-ray emission decay times from nuclear reactions between fusion alphas and beryllium impurities ($^{9}Be(\alpha,n\gamma)^{12}C$) are consistent with classical alpha (and parent triton) slowing down times for high plasma currents (I_p >2MA) and monotonic q-profiles. γ-ray emission decay times are much shorter in CH plasmas, indicating alpha confinement degradation and spatial redistribution, due to the effect of enlarged orbits, predicted by the 3-D Fokker Planck code.

ACKNOWLEDGEMENT

This work was performed under the European Fusion Development Agreement, and funded partly by the UK Engineering and Physical Sciences Research Council and by EURATOM.

REFERENCES

[1]. The JET Team, Nucl. Fusion 32 (1992) 187.
[2]. M. Keilhacker, Phil.Trans.R.Soc.London A **357** (1999) 415.
[3]. G.F. Matthews, et al., J. Nucl. Mater. **266-269** (1999) 153
[4]. The JET Team, presented by K-D. Zastrow, Nucl. Fusion **39** (1999) 1891
[5]. P. Efthimion, et al., Phys. Rev. Letters **55** (1995) 85
[6]. P. Efthimion, et al., Nucl. Fusion **39** (1999) 1905
[7]. A. Murari, et al., in Fusion Energy 2004 (Proc. 20th Int.Conf. Vilamoura, 2004) (Vienna: IAEA) CD-ROM File OV/P4-9. http://www-naweb.iaea.org/napc/physics/fec/fec2004/datasets/index.html
[8]. T.T.C. Jones, et al., Fusion Science and Technology **48** (2005) 250
[9]. S. Popovichev, et al., "Performance of Neutron Measurements during Trace Tritium Experiments on JET", Proc. 31st EPS Conference on Plasma Physics, London 2004, P5-173
[10]. P. Andrew, et al., Fus Eng and Design **47** (1999) 233.
[11]. L. Bertalot, et al., "ITER relevant developments in neutron diagnostics during the JET Trace Tritium Campaign", Proc. 23rd Symposium on Fusion Technology, Venice, 2004.
[12]. K-D. Zastrow, et al., Plasma Phys. and Contr. Fusion **46** (2004) B255.
[13]. L. Lauro-Taroni, et al., "Impurity transport in High Performance discharges in JET", Proc 21st EPS Conference on Controlled Fusion and Plasma Physics, Montpellier, vol.1, p102.
[14]. R. Goldston, et al., J. Comput. Phys. **43** (1994) 93
[15]. A.D. Whiteford, et al., "Quantitative forward modelling of neutron emission to derive transport coefficients of tritium in JET including error propagation through to transport parameters", Proc 31st EPS Conference on Plasma Physics, London 2004, P1-159.
[16]. W.A. Houlberg, et al., Nucl. Fusion **34** (1994) 93

[17]. I. Voitsekhovitch, et al., “Transport analysis of trace Tritium experiments on JET and comparison with theory-based transport models”, Proc. 31st EPS Conference on Plasma Physics, London 2004, P1-158

[18]. D.C. McDonald, et al, in Fusion Energy 2004 (Proc. 20th Int.Conf. Vilamoura, 2004) (Vienna: IAEA) CD-ROM File EX/6-6. . http://www-naweb.iaea.org/napc/physics/fec/fec2004/datasets/index.html

[19]. C.C. Petty, et al., Phys. Plasmas **11** (2004) 2514

[20]. A.C.C. Sips, et al., Plasma Phys and Controlled Fusion **44** (2002) B69

[21]. T.C. Luce, et al., Nuclear Fusion **43** (2003) 321

[22]. E. Joffrin, et al., in Fusion Energy 2004 (Proc. 20th Int.Conf. Vilamoura, 2004) (Vienna: IAEA) CD-ROM File EX/4-2. . http://www-naweb.iaea.org/napc/physics/fec/fec2004/datasets/index.html

[23]. A.A. Tucillo, et al., in Fusion Energy 2004 (Proc. 20th Int.Conf. Vilamoura, 2004) (Vienna: IAEA) CD-ROM File EX/1-1. http://www-naweb.iaea.org/napc/physics/fec/fec2004/datasets/index.html

[24]. J. Mailloux, et al., “Tritium Fuelling of JET plasmas with Internal Transport Barriers”, Proc. 31st EPS Conference on Plasma Physics, London 2004, P1-148

[25]. J .W. Connor, and Taylor, J. B., Nucl. Fusion **17** (1977) 1047

[26]. P. Belo, et al., “Role of impurity and deuterium fuelling in evolution of trace tritium in JET ELMy H-mode: transport analysis and predictive modelling”, Proc. 31st EPS Conference on Plasma Physics, London 2004, P1-169

[27]. T.C. Hender, et al., “Trace-Tritium Measurement of Magnetic Island Effect on Particle Confinement”, Proc. 31st EPS Conference on Plasma Physics, London 2004, P1-163

[28]. V. Kiptily, et al., Phys.Rev.Letters **93**(11) (2004) 115001

[29]. N.C. Hawkes, et al., Phys.Rev.Letters **87** (2001) 115001

[30]. V. Yavorskij, et al., in Fusion Energy 2004 (Proc. 20th Int.Conf. Vilamoura, 2004) (Vienna: IAEA) CD-ROM File TH/P4-49. . http://www-naweb.iaea.org/napc/physics/fec/fec2004/datasets/index.html

[31]. N.C. Hawkes., et al., “Tritium fast ion distribution in JET current hole plasmas”, in preparation for Plasma Phys and Controlled Fusion.

[32]. V. Yavorskij, et al., Nucl. Fusion **44**(3) (2004) L5-L10.

[33]. D.N. Borba et al., Nucl. Fusion **40** (2000) 775

[34]. S.E. Sharapov, et al., “Experiment on tritium beam evolution in JET plasmas with Fishbones and TAE mode.”, Proc. 31st EPS Conference on Plasma Physics, London 2004, P5-166

[35]. R. Aymar, et al., Plasma Phys and Controlled Fusion **44** (2002) 519

[36]. B.J. Green, et al., Plasma Phys and Controlled Fusion **45** (2003) 687

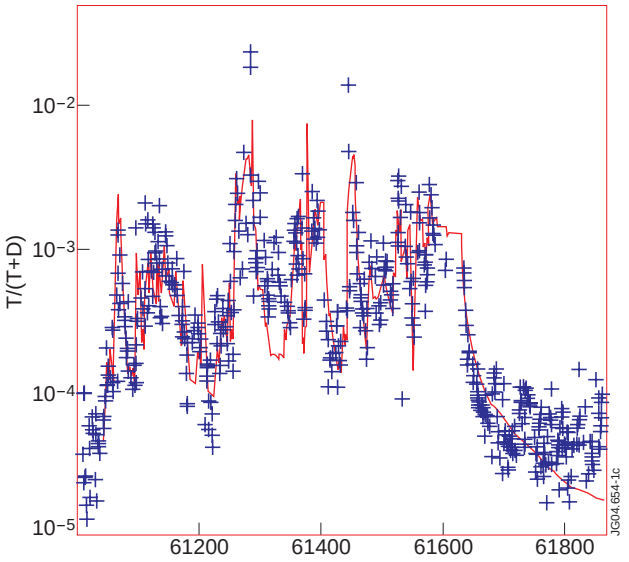

Figure 1: Shot to shot variation in tritium concentration in TTE plasmas as measured from 14MeV and 2.5MeV neutron ratios (+) and compared to the model prediction (solid line) based on a modification of the JET PTE model [10].

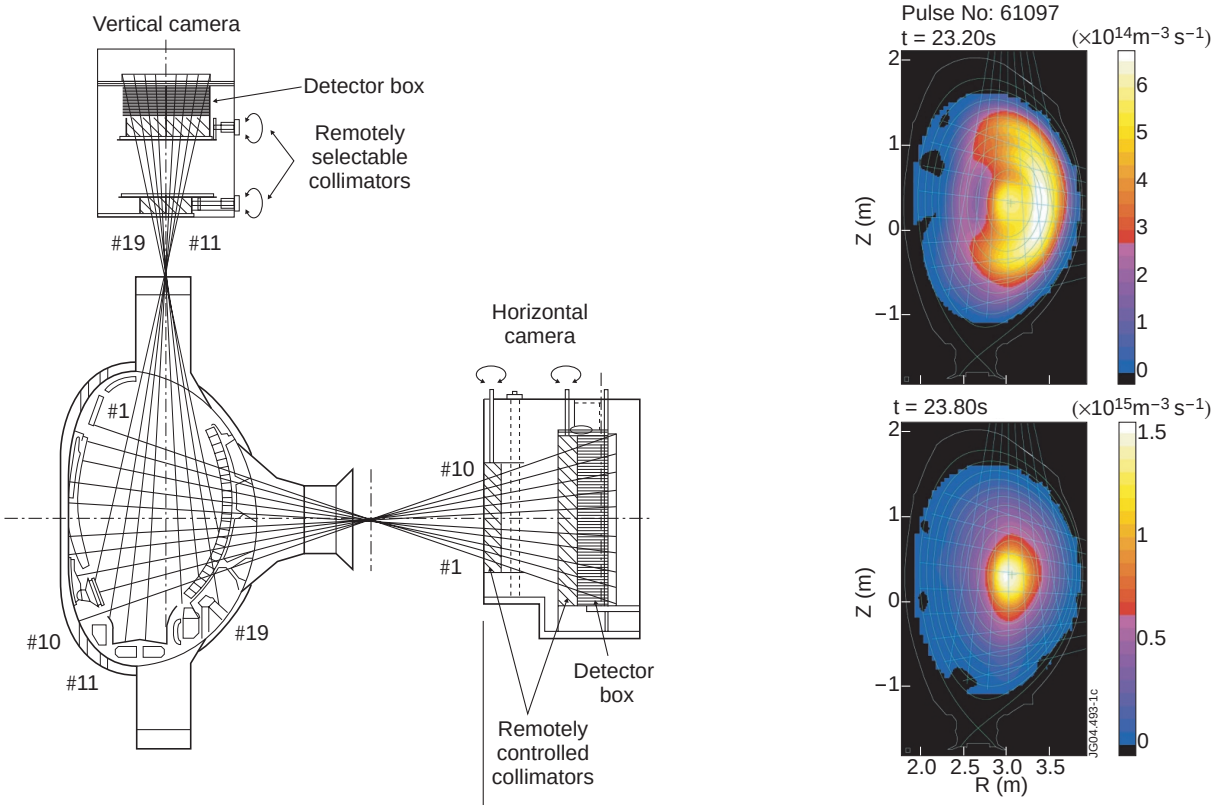

Figure 2: (Left) Schematic overview of the JET neutron camera, showing lines of sight. (Right) Comparison of 14MeV emissivity contours for a shot with tritium gas puff. Top figure shows contours 150ms after the puff, when the tritium density is hollow. Bottom figure shows peaked shape after 750ms once the tritium density profile has relaxed. Initial crescent shape is due to the poloidal distribution of fast NBI deuterium ions.

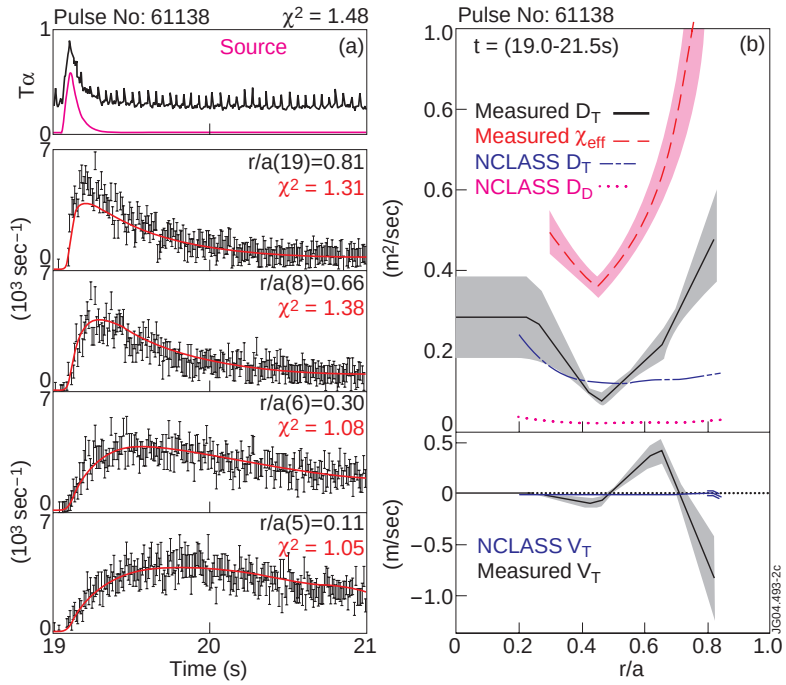

Figure 3: (a) Time evolution of the 14 MeV neutron signal in four individual chords of the neutron profile monitor, covering the range from the edge of the observed region to the core. The top frame shows the T_α input signal from the tritium gas puff. The fits to the data are shown (note all 19 camera channels are entered in the fit). (b) Tritium diffusion and convection coefficients for the fit to the high-density ELMy H-mode shot shown in (a), with comparison to the neoclassical predictions from NCLASS [16]. Shaded areas indicate the confidence limits for the fitted quantities. Note that the NCLASS prediction is for the proper trace tritium quantity, and can be directly compared to the measurement. The ratio of the NCLASS predictions for D_T/D_D is larger than the simple neoclassical $(m_T/m_D)^{1/2}$ because of the trace nature of the tritium and the presence of impurities (see text).

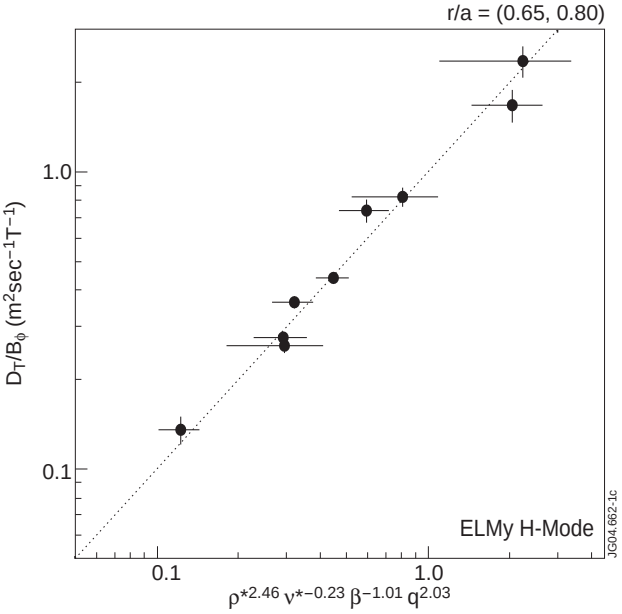

Figure 4: Experimentally-derived normalised diffusion coefficient (D_T/B_ϕ) for the plasma region 0.65 <r/a < 0.8 for a set of NBI-heated NTM-free ELMy H-modes plotted against a fit to the data as a power law product of ρ, ν*, β and q.*

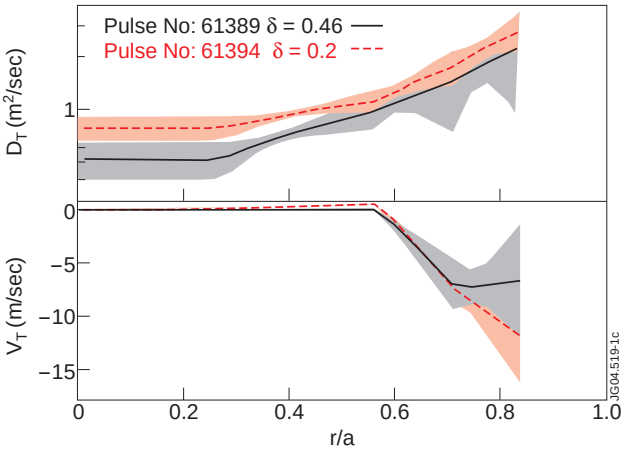

Figure 5: Fitted tritium diffusion coefficient (D_T) and convective velocity (v_T) spatial profiles for two hybrid scenario discharges at different triangularities. The discharges were performed at the same Ip and B_T, and the gain $G=H\beta_N/q_{95}^2$ ~ 0.32 was approximately constant for the two plasmas.

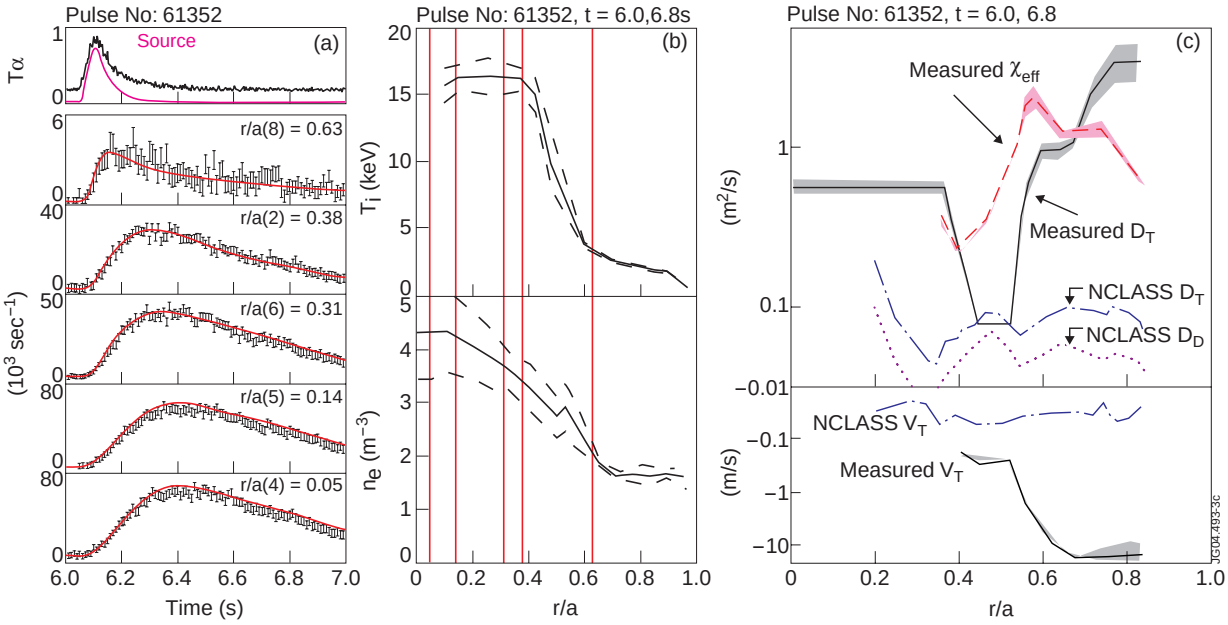

Figure 6: Tritium transport data and fits for a discharge with strong ITB and tritium gas puff.
(a) Tritium gas source (via Tα measurement – top trace) and 14MeV neutron signal time development for selected camera channels.
(b) Ion temperature and electron density profiles for the ITB discharge with strong barrier present - vertical lines mark the radial positions of the camera channels in (a).
(c) Fitted tritium diffusion coefficient and convective velocity spatial profiles for ITB discharge compared to neo-classical predictions from NCLASS code [16].

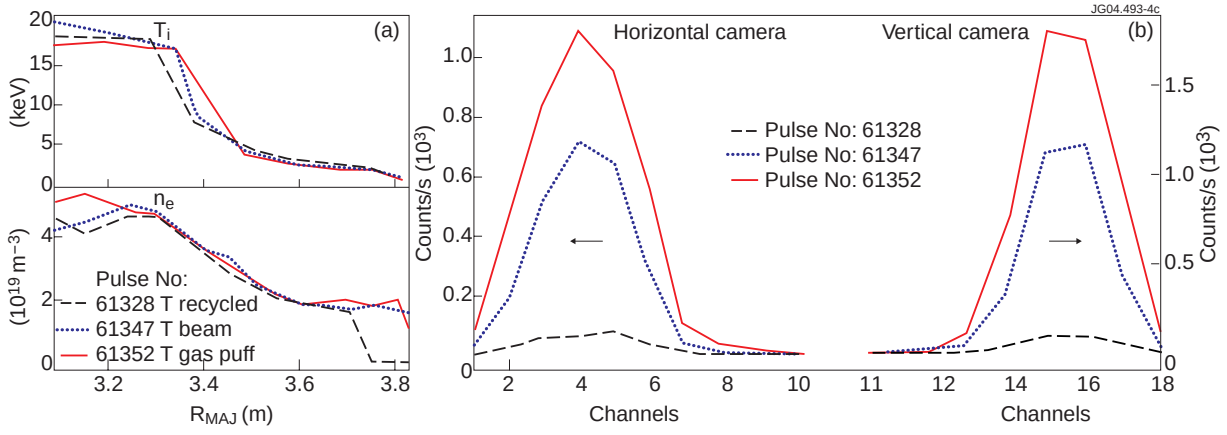

Figure 7: (a) Ion temperature and electron density profiles for three identical ITB discharges, two with tritium transient fuelling provided by T gas puff (Pulse No: 61352) and T^0 NBI (Pulse No: 61347) the third with tritium wall recycling only (Pulse No: 61328). (b) 14MeV neutron camera profiles compared for the three shots, at the time of the profiles in (i). At these times, for the transient shots, the T^0 NBI fast ions have slowed down (Pulse No: 61347) or the T ions from gas puff have reached the plasma core (Pulse No: 61352).

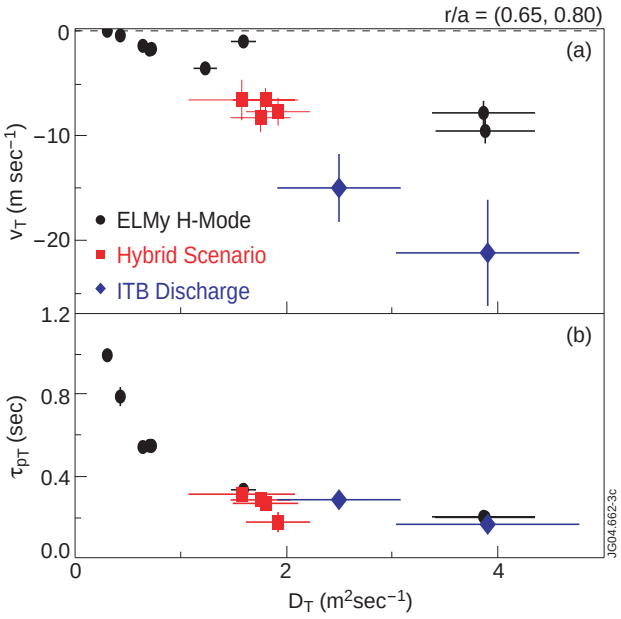

Figure 8: (a) Plot of derived tritium convective velocity (v_T) against tritium diffusion coefficient (D_T) for the NBI heated ELMy H-modes, the Hybrid scenarios pulses and the ITB pulses. (b) Tritium particle confinement time (τ_{pT}) plotted against tritium diffusion coefficient for the dataset in Fig.8(a). The value of τ_{pT}* is obtained from the decay of the 14MeV DT neutrons following the thermalisation of a T^0 NBI beam pulse injected into the deuterium plasmas.*

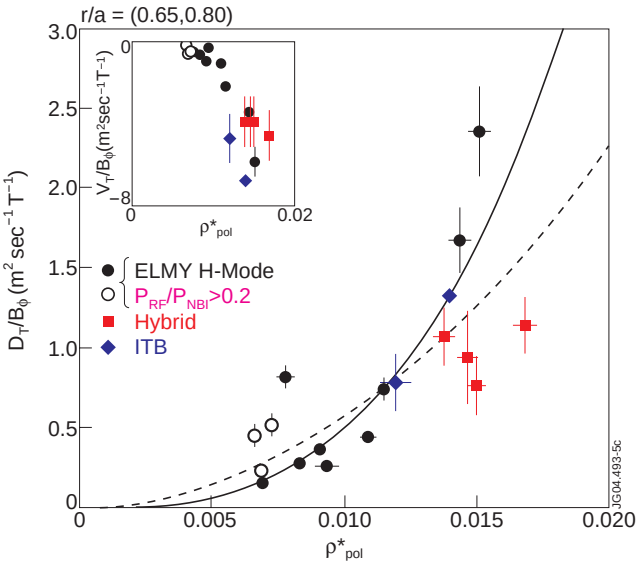

Figure 9: Plot of normalised D_T/B_ϕ and v_T/B_ϕ against local poloidal Larmor radius ($\rho^*_{pol}=q\times\rho^*$) for 0.65<r/a<0.8 in various JET discharge regimes. The solid line corresponds to Gyro-Bohm scaling (ρ^{*3}_{pol}), the dashed line to Bohm scaling (ρ^{*2}_{pol}).

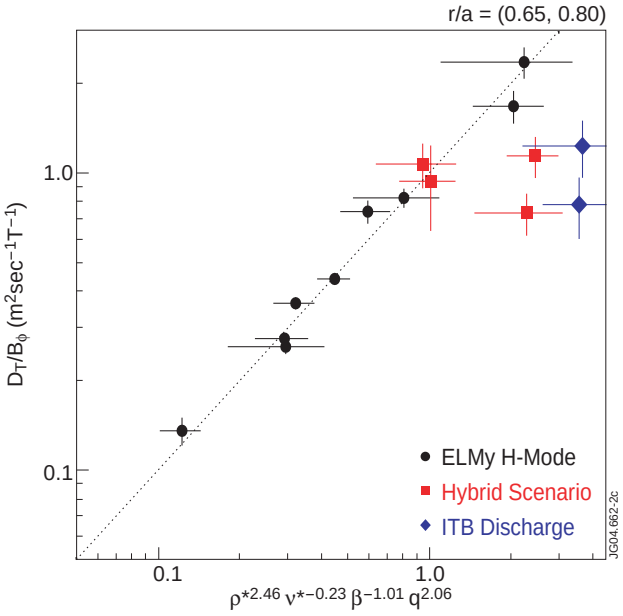

Figure 10: Experimentally derived normalized diffusion coefficients (D_T/B_ϕ) for the various regimes plotted against the multiparameter fit to the ELMy H-modes only.

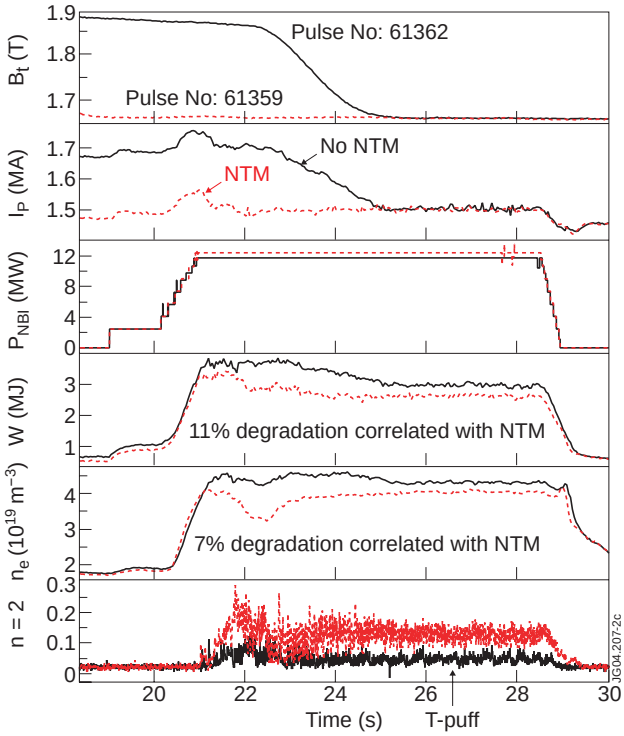

Figure 11: Time traces for two ELMy H-modes: one without any strong NTM activity (Pulse No: 61362) and one where the pulse conditions were prepared to generate strong 3/2 NTM activity (Pulse No: 61359). Tritium gas was puffed into both pulses as indicated at t = 26.5s. during a phase where discharge parameters were kept constant until t = 28.5s.

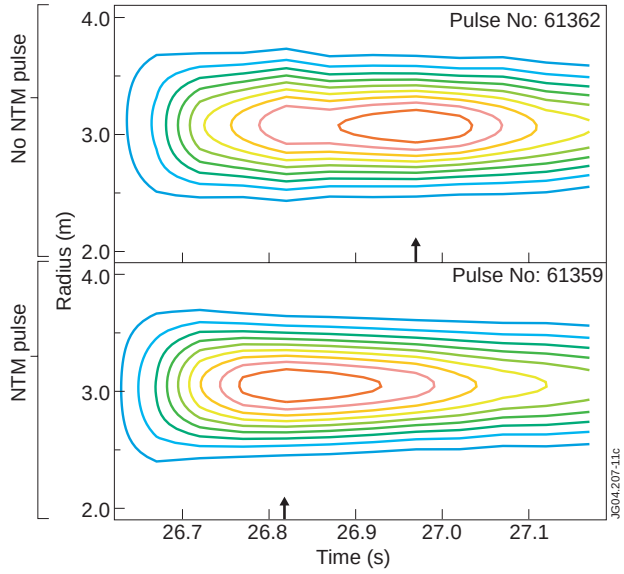

Figure 12: Time history of the 14MeV neutron radial emissivity contours following the tritium puff at t = 26.5s. for the discharge with NTM (Pulse No:61359) and without NTM (Pulse No:61362). The time of peaking of the plasma tritium profile is indicated by the arrows. The faster transit of the tritium to the plasma centre in the NTM case is evident.

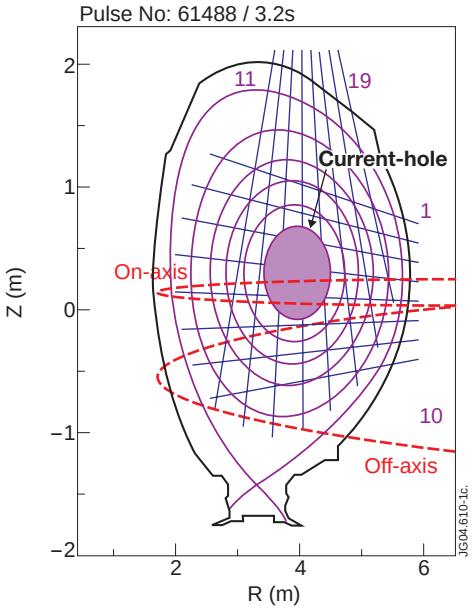

Figure 13: Poloidal cross section of JET Current Hole (CH) discharge showing:
- extent of current hole;
- poloidal projections of on-axis and off-axis T^0 NBI trajectories (red dashed lines); and
- neutron camera lines of sight.

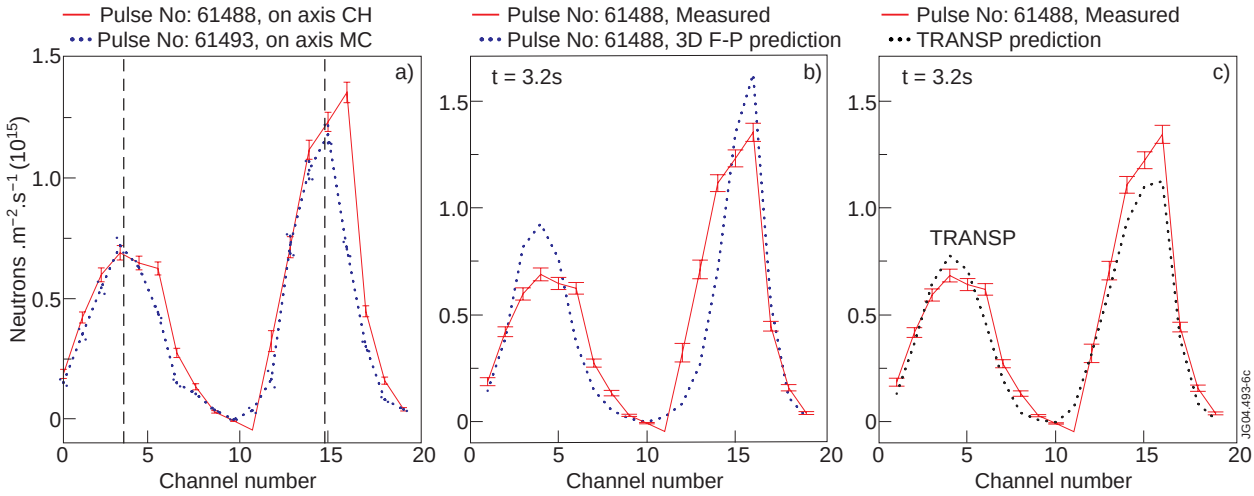

Figure 14: (a) Neutron emission profiles from the vertical and horizontal cameras for on-axis T^0 NB injection in the case of current hole(CH) and monotonic current (MC) profile plasmas. Vertical dashed lines indicate the axis of the plasma for the two views. (b) Comparison of Fokker Planck (F-P) code prediction for neutron profiles and neutron camera data for the case of on-axis injection into the CH discharge. (c) Comparison of TRANSP code prediction for neutron profiles and neutron camera data for the same on-axis injection case as in (b). Measurements and predictions correspond to the end of 200ms NBI pulses.

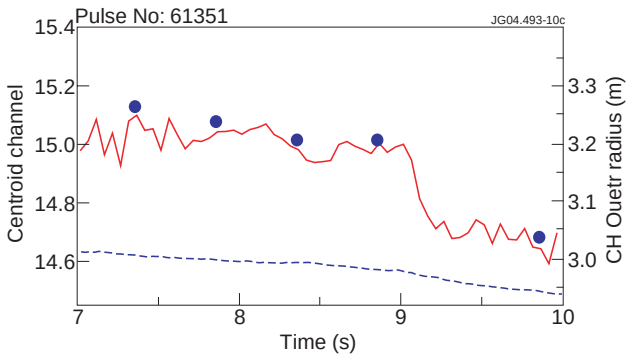

Figure 15: Centroid movement for 14MeV neutron emission profile (solid line) superimposed on the shrinkage of the current hole (circles). Dashed line shows the magnetic axis position.

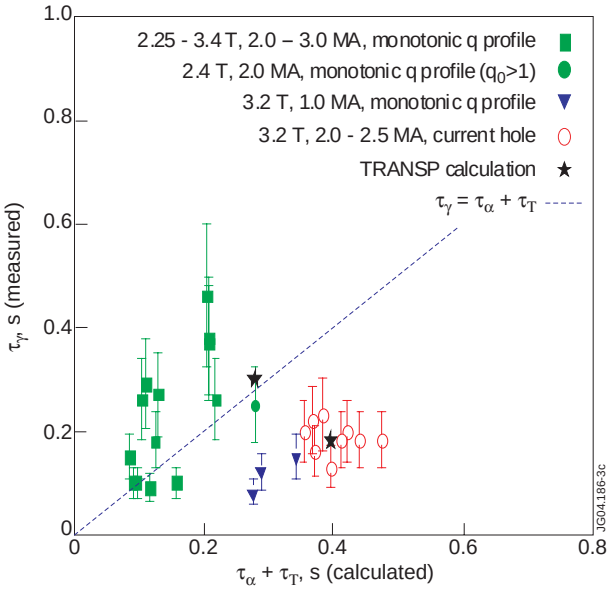

Figure 16: Measured 4.44-MeV gamma-ray decay-times due to the Be+alpha nuclear reaction vs. calculated classical slowing down-times of T-beam ions and alpha particles for plasma scenarios with: B_T=2.25-3.2T, I_p=1.0-3.0MA. The TRANSP simulations (starred points) were perfomed for the nearby Hybrid scenario point (star near the dashed equality line) and for a nearby Current Hole plasma (star in the centre of the Current Hole data).

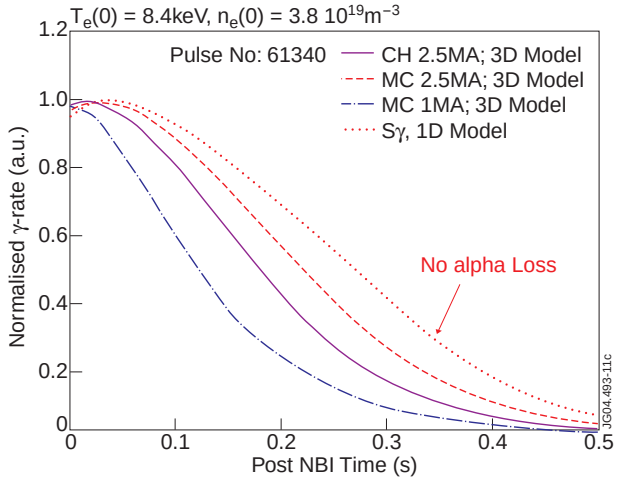

Figure 17: Normalised γ-decay rate (post T-NBI) from 3-D Fokker Planck (F-P) code simulation for I_p=2.5MA Current Hole (CH) Pulse No:61340, with central parameters as shown and CH radius ρ_*/a ~0.57(solid curve). Dashed curves are 3-D F-P results for Monotonic Current (MC) plasmas with same T_e, n_e profiles and I_p as shown. Dotted curve shows 1-D F-P model for I_p=2.5MA MC plasma.